# Catalysis by Oxide-Supported Clusters of Iridium and Rhodium: Hydrogenation of Ethene, Propene, and Toluene

**A. M. Argo, J. F. Odzak, J. F. Goellner, F. S. Lai, F.-S. Xiao, and B. C. Gates***

*Department of Chemical Engineering and Materials Science, University of California, Davis, California 95616*

*Received: August 27, 2005; In Final Form: December 4, 2005*

The hydrogenation reactions of ethene, propene, and toluene were used as probes of the catalytic properties of small clusters of rhodium ($Rh_6$) and of iridium ($Ir_4$ and $Ir_6$) (as well as of larger aggregates of these metals) on oxide supports ($\gamma$-$Al_2O_3$, MgO, and $La_2O_3$). The catalysts were characterized in the working state by extended X-ray absorption fine structure (EXAFS) spectroscopy, providing evidence of the cluster structures and cluster-support interactions; by infrared spectroscopy, providing evidence of hydrocarbon adsorbates and possible reaction intermediates on the clusters; and by kinetics of the hydrogenation reactions. The EXAFS data indicate that the metal clusters, while remaining intact and maintaining their bonding to the support during catalysis, underwent slight rearrangements to accommodate reactive intermediates. As the concentrations of reactive intermediates such as $\pi$-bonded alkenes and alkyls on the clusters increased, the cluster frames swelled, and the clusters flexed away from the support. The data indicate self-inhibition of reaction by adsorbed hydrocarbons and differences between ethene hydrogenation and propene hydrogenation that may arise primarily from different adsorbate−adsorbate interactions.

## Introduction

The hydrogenation reactions of small alkenes[1,2] and aromatics[2,3] are good probes of the catalytic properties of metals when the structures containing the metals are so small as to limit the structure and bonding of the probe molecule. In earlier work that is part of the foundation of the present report,[4] we investigated oxide-supported catalysts that are well approximated as $Ir_4$, $Ir_6$, and $Rh_6$ for hydrogenation of ethene and of propene, characterizing the catalysts in the functioning state by extended X-ray absorption fine structure (EXAFS) spectroscopy to provide evidence of the structures of the clusters and their interactions with the supports and by infrared (IR) spectroscopy to provide evidence of adsorbates (ligands) on the clusters. Here we extend the investigation to toluene hydrogenation as a further test reaction and add kinetics data to complement the spectroscopy reported earlier and provide a basis for comparing the reactivities of ethene, propene, and toluene.[5] The goal was to elucidate patterns of reactivity as a function of reactant size and structure and to understand better how metal cluster properties affect the catalysis.

## Experimental Methods

Details of the catalyst synthesis are reported elsewhere; the catalysts include oxide-supported iridium clusters $Ir_4/\gamma$-$Al_2O_3$,[6] $Ir_4$/MgO,[7] and $Ir_6/\gamma$-$Al_2O_3$[8] as well as structurally nonuniform samples formed by aggregation of the metals in these samples, namely, $Ir_{agg}/\gamma$-$Al_2O_3$[9] and $Ir_{agg}$/MgO;[5] other samples include $Rh_6/\gamma$-$Al_2O_3$,[10] $Ir_6$/MgO,[11] $Rh_6$/MgO,[12] and $Rh_6/La_2O_3$.[13,14] (The subscript agg refers to aggregated clusters.)

Sample handling was carried out on a vacuum line or in a glovebox (Vacuum Atmospheres HE-63-P) purged with $N_2$ that was recirculated through $O_2$- and moisture-scavenging traps (supported copper particles and zeolite 4A, respectively). The glovebox was equipped with $O_2$ and moisture detectors, indicating concentrations < 2 ppm of each. Toluene (99.7%, J. T. Baker) was degassed by sparging with $N_2$ (99.997%, Liquid Carbonic) before use. He (Matheson, 99.999%), ethene (Matheson, 99.5%), and propene (Matheson, 99.5%) were purified by passage through traps to remove traces of $O_2$ and moisture. $H_2$ was supplied by Matheson (99.999%) or generated by electrolysis of water in a Balston generator (99.99%) and purified by traps. Samples contained 1.0 wt % metal, with the exception of $Rh_6/La_2O_3$, which contained 0.5 wt % Rh.

Measurements of the catalytic activity for hydrogenation of ethene, propene, or toluene were carried out with a conventional once-through tubular flow reactor operated at atmospheric pressure and temperatures ranging from 233 to 373 K. Details of these experiments are described elsewhere.[8,14,15]

The standard conditions chosen to compare the catalysts for alkene hydrogenation were as follows: alkene partial pressure, 40 Torr; $H_2$ partial pressure, 100 Torr; and temperature 294 ± 1 K. In kinetics experiments, the $H_2$ partial pressure was varied from 50 to 400 Torr and the alkene partial pressures from 10 to 300 Torr. Standard toluene hydrogenation experiments were carried out with a toluene partial pressure ($P_{C7H8}$) of 50 Torr and a hydrogen partial pressure ($P_{H2}$) of 710 Torr at 333 K. In kinetics experiments, these partial pressures were varied in the ranges of 10−50 and 140−710 Torr, respectively. The reaction rates were determined from differential conversions with an accuracy of about ±10%.[15]

Details of the X-ray absorption spectroscopy experiments are described elsewhere[12] as is the EXAFS cell that served as a flow reactor.[16] Toluene-containing gaseous feeds to the EXAFS cell/reactor were produced by bubbling He through a saturator containing liquid toluene at room temperature.

The range of hydrocarbon conversions in the EXAFS cell/reactor was 0.01−0.98. When the conversions were relatively high, there were significant concentration gradients across the

* To whom correspondence should be addressed. E-mail bcgates@ucdavis.edu.

10.1021/jp0548523 CCC: $33.50 
Published on Web 01/11/2006

**TABLE 1: Catalytic Activities for Ethene Hydrogenation, Propene Hydrogenation, and Toluene Hydrogenation under Standard Conditions[a]**

| | 10 × reaction rate, mol/(mol of metal × $s^{-1}$) | | |
|---|---|---|---|
| catalyst | ethene hydrogenation[a] | propene hydrogenation[b] | toluene hydrogenation[c] |
| $Ir_4/\gamma\text{-}Al_2O_3$ | 0.91 | 0.59 | 0.0094[5] |
| $Ir_6/\gamma\text{-}Al_2O_3$ | 0.29 | – | 0.017[8] |
| $Ir_{Agg}/\gamma\text{-}Al_2O_3$ | 0.89 | 1.07 | 0.099[5] |
| $Ir_4$/MgO | 0.17 | 0.26 | 0.0059[1] |
| $Ir_6$/MgO | 0.15 | – | 0.0023 |
| $Ir_{Agg}$/MgO | 0.15 | – | 0.020[5] |
| $Rh_6/\gamma\text{-}Al_2O_3$ | 0.65 | – | 0.084 |
| $Rh_6$/MgO | 0.96 | – | 0.078 |
| $Rh_6/La_2O_3$ | 3.7 | – | 0.23 |

[a] Reaction at 620 Torr of He, 100 Torr of $H_2$, and 40 Torr of $C_2H_4$ at 273 K. [b] Reaction at 620 Torr of He, 100 Torr of $H_2$, and 40 Torr of $C_3H_6$ at 273 K. [c] Reaction at 710 Torr of $H_2$ and 50 Torr of $C_7H_8$ at 333 K.

**TABLE 2: Apparent Activation Energies for Ethene Hydrogenation, Propene Hydrogenation, and Toluene Hydrogenation at Standard Reactant Partial Pressures[a]**

| | apparent activation energy, kJ/mol | | |
|---|---|---|---|
| catalyst | ethene hydrogenation | propene hydrogenation | toluene hydrogenation |
| $Ir_4/\gamma\text{-}Al_2O_3$ | 24.3 | 34.2 | 48[5] |
| $Ir_6/\gamma\text{-}Al_2O_3$ | 28.6 | – | 38[8] |
| $Ir_{Agg}/\gamma\text{-}Al_2O_3$ | 28.2 | 33.1 | 55[5] |
| $Ir_4$/MgO | 38.5 | 34.8 | 58.2 |
| $Ir_6$/MgO | 38.4 | – | 56.5 |
| $Ir_{Agg}$/MgO | 31.5 | – | 55[5] |
| $Rh_6/\gamma\text{-}Al_2O_3$ | 29.7 | – | 37.4 |
| $Rh_6$/MgO | 40.7 | – | 42.1 |
| $Rh_6/La_2O_3$ | 94.4 | – | 31.2 |

[a] See Table 1 for reactant partial pressures and text for ranges of temperature.

portion of the catalyst bed characterized by EXAFS spectroscopy, and the results are only qualitatively comparable to those obtained in the conventional flow reactor (otherwise, the comparisons were quantitative; details are given elsewhere[14]). Although the catalytic reactions are exothermic, there is no evidence of significant effects, such as hot-spot formation, on the EXAFS data.

### Analysis of EXAFS Data

Details of the EXAFS data analysis have been described elsewhere,[12] and Supporting Information Tables 1 and 2 provide some relevant information.[17−25]

## Results

**Rates of Hydrogenation of Ethene, Propene, and Toluene.** In ethene hydrogenation catalysis by oxide-supported metal clusters under our conditions (e.g., 273 K; $P_{H2}$, 100 Torr; $P_{ethene}$, 40 Torr; $P_{He}$, 620 Torr), the only observed product was ethane. There was no measurable conversion in the absence of catalyst. Similar statements pertain to experiments with propene (giving propane) and toluene (giving methylcyclohexane). The steady-state catalytic activities are reported per total noble metal atom in the sample; when the catalysts consist of small clusters (such as $Ir_4$ or $Ir_6$) in which essentially all the metal atoms are exposed, these rates correspond to turnover frequencies (TOF).

Partial results have been communicated, including rates of catalytic hydrogenation of ethene and of propene catalyzed by $Ir_4/\gamma\text{-}Al_2O_3$ and by $Ir_4$/MgO;[4,26,14] of ethene by $Ir_6$/MgO, $Rh_6$/MgO,[12,14] $Ir_4/\gamma\text{-}Al_2O_3$, and $Ir_6/\gamma\text{-}Al_2O_3$;[27,14] and of toluene by $Ir_4$/MgO, $Ir_6$/MgO, $Ir_{Agg}$/MgO,[1,5] $Ir_6/\gamma\text{-}Al_2O_3$,[8] and $Ir_4/\gamma\text{-}Al_2O_3$.[5] The activities of each catalyst for hydrogenation of ethene and of propene at $P_{H2} = 100$ Torr and $P_{hydrocarbon} = 40$ Torr at 273 K and for toluene at $P_{H2} = 710$ Torr and $P_{toluene} = 50$ Torr at 333 K are summarized in Table 1.

The data indicate the following: $\gamma\text{-}Al_2O_3$-supported iridium catalysts are substantially more active than MgO-supported iridium catalysts, and $\gamma\text{-}Al_2O_3$- and MgO-supported rhodium cluster catalysts (i.e., $Rh_6$ but not aggregates of rhodium clusters) are slightly more active than the most active iridium catalysts (supported aggregates of iridium). The $La_2O_3$-supported rhodium catalyst is approximately four times as active as the most active MgO- or $\gamma\text{-}Al_2O_3$-supported rhodium or iridium catalyst.[13,14]

The data demonstrate that whereas ethene hydrogenation and propene hydrogenation on iridium clusters or aggregates take place at approximately equal rates, toluene hydrogenation is an order of magnitude faster on iridium aggregates than on iridium clusters. In contrast, ethene is hydrogenated at similar rates on $Rh_6$ (supported on $\gamma\text{-}Al_2O_3$ or MgO) and on iridium aggregates, and toluene is hydrogenated at similar rates on $Rh_6$ (supported on $\gamma\text{-}Al_2O_3$ or MgO) and on iridium aggregates.

**Apparent Activation Energies.** The apparent activation energies (determined by the dependence of the catalytic reaction rate on temperature) for each reaction with each catalyst are summarized in Table 2. The data show that the hydrogenation of the alkenes on supported metal clusters, like that on extended metal surfaces,[28−31] is characterized by apparent activation energies (typically 24−40 kJ $mol^{-1}$) that are less than those observed for toluene hydrogenation[5] (typically 41−56 kJ $mol^{-1}$).

**Reaction Orders.** At 273 K and low alkene partial pressures ($P_{alkene}$), the reaction orders in $H_2$ range from 0.6 to 0.7, being similar for the hydrogenation of ethene and the hydrogenation of propene on iridium (Tables 3−5, Figures 1A and 2A). In contrast, the reaction orders in $H_2$ are close to 1.0 for toluene hydrogenation (at 333 K and 50 Torr of toluene). The reaction orders in $H_2$ for ethene hydrogenation on rhodium clusters, on the other hand, are greater than 1.0 under similar conditions.

At low values of the alkene partial pressure, the orders in alkene for reaction catalyzed by supported metal clusters and aggregates are slightly negative (Tables 3 and 5, Figures 1B and 2B) and similar in value for ethene and propene. However, at higher values of these partial pressures ($P_{ethene}$ of 150−200 Torr for ethene hydrogenation and $P_{propene}$ of 75−100 Torr for propene hydrogenation), the reaction order in alkene is greater—approximately zero—whereas at $P_{alkene}$ exceeding these pivotal partial pressures ($P_p$), the order in alkene is approximately unity. Such a change in reaction order has been reported before for hydrogenation of ethene and of propene catalyzed by conventional supported metals[28−30,32] as well as supported metal clusters.[4,12,14,26,27]

In contrast, the reaction order in toluene is slightly positive for $P_{toluene} > 10$ Torr, indicating a qualitative difference between alkene and arene hydrogenation on supported metal clusters and aggregates.

**Influence of Temperature on Reaction Orders for Propene Hydrogenation.** Further evidence of the contrast between propene hydrogenation at low and high values of $P_{propene}$ is the following: As the temperature increased from 253 to about 290 K at a low value of $P_{propene}$ (52 Torr), the order in $H_2$ increased from 0.6 to 1.0 for the reaction on $Ir_4/\gamma\text{-}Al_2O_3$ and from 0.7 to 0.8 for the reaction on $Ir_4$/MgO (Table 4). In contrast, at high values of $P_{propene}$ (> 100 Torr), as the temperature increased from 253 to about 290 K at $P_{H2} = 313$ Torr, the order in propene

**TABLE 3: Reaction Orders in $H_2$ and in Hydrocarbon (HC) for Catalytic Hydrogenation of Ethene, Propene, and Toluene on Oxide-Supported Iridium Clusters and Rhodium Clusters**

| catalyst | hydrocarbon (HC) reactant | $T$, K | (range of) $P_{H2}$, Torr | (range of) $P_{HC}$, Torr | reaction order in $H_2$ | reaction order in HC | reference for more details |
|---|---|---|---|---|---|---|---|
| $Ir_4/\gamma$-$Al_2O_3$ | ethene | 273 | 50−300 | 40 | 0.68 | − | 27 |
| $Ir_4/\gamma$-$Al_2O_3$ | propene | 273 | 50−400 | 40 | 0.66 | − | − |
| $Ir_4$/MgO | ethene | 273 | 50−300 | 40 | 0.69 | − | − |
| $Ir_4$/MgO | propene | 273 | 54−364 | 52 | 0.69 | − | − |
| $Ir_4$/MgO | toluene | 373 | 140−710 | 49 | 1.07 | − | − |
| $Ir_6/\gamma$-$Al_2O_3$ | ethene | 273 | 50−300 | 40 | 0.6 | − | 27 |
| $Ir_6$/MgO | ethene | 273 | 50−300 | 40 | 0.68 | − | 12 |
| $Ir_6$/MgO | toluene | 373 | 140−710 | 50 | 0.85 | − | −1 |
| $Ir_{Agg}/\gamma$-$Al_2O_3$ | ethene | 273 | 50−300 | 40 | 0.83 | − | 27 |
| $Ir_{Agg}/\gamma$-$Al_2O_3$ | propene | 273 | 50−300 | 40 | 0.71 | − | − |
| $Ir_{Agg}$/MgO | ethene | 273 | 50−300 | 40 | 1.52 | − | − |
| $Ir_{Agg}$/MgO | toluene | 373 | 140−710 | 50 | 0.92 | − | − |
| $Rh_6/\gamma$-$Al_2O_3$ | ethene | 273 | 50−300 | 40 | 1.24 | − | − |
| $Rh_6$/MgO | ethene | 273 | 50−300 | 40 | 1.47 | − | 12 |
| $Rh_6/La_2O_3$ | ethene | 273 | 50−300 | 40 | 1.71 | − | − |
| $Ir_4/\gamma$-$Al_2O_3$ | ethene | 273 | 300 | 40−200 | − | −0.25 | 27 |
| $Ir_4/\gamma$-$Al_2O_3$ | propene | 273 | 300 | 100−300 | − | 1.24 | − |
| $Ir_4/\gamma$-$Al_2O_3$ | propene | 273 | 100 | 10−75 | − | −0.28 | − |
| $Ir_4$/MgO | ethene | 273 | 300 | 40−150 | − | −0.22 | − |
| $Ir_4$/MgO | propene | 273 | 313 | 154−310 | − | 1.4 | − |
| $Ir_4$/MgO | toluene | 373 | 710 | 10−50 | − | 0.12 | − |
| $Ir_6/\gamma$-$Al_2O_3$ | ethene | 273 | 300 | 40−150 | − | −0.18 | 27 |
| $Ir_6/\gamma$-$Al_2O_3$ | ethene | 273 | 400 | 250−360 | − | 0.75 | − |
| $Ir_6$/MgO | ethene | 273 | 300 | 40−150 | − | −0.12 | 12 |
| $Ir_6$/MgO | toluene | 373 | 710 | 10−50 | − | 0.13 | − |
| $Ir_{Agg}/\gamma$-$Al_2O_3$ | ethene | 273 | 300 | 40−150 | − | −0.27 | 27 |
| $Ir_{Agg}$/MgO | ethene | 273 | 300 | 40−150 | − | −0.28 | − |
| $Ir_{Agg}$/MgO | toluene | 373 | 710 | 10−50 | − | 0.1 | − |
| $Rh_6/\gamma$-$Al_2O_3$ | ethene | 273 | 300 | 40−100 | − | −0.21 | − |
| $Rh_6$/MgO | ethene | 273 | 300 | 40−150 | − | −0.2 | 12 |
| $Rh_6/La_2O_3$ | ethene | 273 | 300 | 40−100 | − | −0.21 | − |

**TABLE 4: Influence of Temperature on $H_2$ and Hydrocarbon (HC) Reaction Orders for Propene Hydrogenation on Oxide-Supported $Ir_4$ Clusters**

| catalyst | $T$, K | (range of) $P_{H2}$, Torr | (range of) $P_{HC}$, Torr | reaction order in $H_2$ | reaction order in HC |
|---|---|---|---|---|---|
| $Ir_4/\gamma$-$Al_2O_3$ | 253 | 54−364 | 52 | 0.57 | − |
| $Ir_4/\gamma$-$Al_2O_3$ | 273 | 54−313 | 52 | 0.96 | − |
| $Ir_4/\gamma$-$Al_2O_3$ | 290 | 54−364 | 52 | 1.01 | − |
| $Ir_4$/MgO | 253 | 54−708 | 52 | 0.69 | − |
| $Ir_4$/MgO | 273 | 54−364 | 52 | 0.69 | − |
| $Ir_4$/MgO | 296 | 54−313 | 52 | 0.81 | − |
| $Ir_4/\gamma$-$Al_2O_3$ | 253 | 313 | 200−310 | − | 1.34 |
| $Ir_4/\gamma$-$Al_2O_3$ | 273 | 313 | 154−310 | − | 1.07 |
| $Ir_4/\gamma$-$Al_2O_3$ | 290 | 313 | 154−310 | − | 0.91 |
| $Ir_4$/MgO | 253 | 313 | 154−310 | − | 1.56 |
| $Ir_4$/MgO | 273 | 313 | 154−310 | − | 1.4 |
| $Ir_4$/MgO | 296 | 313 | 154−310 | − | 1.04 |

decreased from 1.3 to 0.9 for the reaction on $Ir_4/\gamma$-$Al_2O_3$ and from 1.6 to 1.0 for the reaction on $Ir_4$/MgO (Table 4).

**Influence of Co-reactant Partial Pressure on Reaction Orders.** The reaction order in $H_2$ increased with increasing $P_{alkene}$ for $P_{alkene}$ below the pivotal pressure $P_p$ for hydrogenation of either ethene or propene on $Ir_4/\gamma$-$Al_2O_3$ or $Ir_6/\gamma$-$Al_2O_3$ at 273 K (Table 5). At $P_{alkene} > P_p$, the order in $H_2$ decreased with increasing $P_{alkene}$ for hydrogenation of ethene and of propene on $Ir_4/\gamma$-$Al_2O_3$ (and $Ir_6/\gamma$-$Al_2O_3$) at 273 K (Table 5). The reaction order in ethene increased from −0.5 to −0.2 with an increase in $P_{H2}$ from 100 to 300 Torr for ethene hydrogenation on $Ir_6/\gamma$-$Al_2O_3$ at 273 K and $P_{ethene} < P_p$ (Table 5). The reaction order in propene decreased from 1.2 to 0.9 with an increase in $P_{H2}$ from 250 to 300 Torr in propene hydrogenation on $Ir_4/\gamma$-$Al_2O_3$ at 273 K and $P_{propene} > P_p$ (Table 5).

**EXAFS Evidence Identifying Oxide-Supported Clusters as Catalytically Active Species.** EXAFS data characterizing $Ir_4/\gamma$-$Al_2O_3$,[4,14,27] $Ir_6/\gamma$-$Al_2O_3$,[14,27] $Ir_4$/MgO,[4,14] $Ir_6$/MgO,[12,14] and $Rh_6$/MgO[12,14] during ethene hydrogenation and characterizing $Ir_4/\gamma$-$Al_2O_3$ and $Ir_4$/MgO during propene hydrogenation[4,14,26] (reported elsewhere, as cited) imply the following about the catalytically active species: (a) because the cluster geometry is maintained during catalysis and the support is catalytically inactive, we infer that the clusters are the catalytically active species, (b) the cluster-support interface and the metal−metal bond distance in the cluster are modified slightly during catalysis, indicating the presence of adsorbates bound to the clusters, and (c) the metal−oxygen coordination shell (with a metal−oxygen distance of approximately 2.1 Å), indicating bonding of the clusters to the support, is reduced slightly during catalysis, indicating that the clusters slightly flex away from the support during reaction.

*$Ir_4/\gamma$-$Al_2O_3$.* EXAFS parameters characterizing $Ir_4/\gamma$-$Al_2O_3$ in flowing He at 298 K and 760 Torr (Table 6) are consistent with the expected tetrahedral $Ir_4$ clusters.[6] EXAFS parameters characterizing $Ir_4/\gamma$-$Al_2O_3$ during toluene hydrogenation at 298 K and 760 Torr (235 Torr of He, 517 Torr of $H_2$, and 8 Torr of toluene) show that the $Ir_4$ cluster structure was essentially unchanged during reaction (Table 6). Because the tetrahedral $Ir_4$ geometry was essentially maintained during catalysis and the support was catalytically inactive, we infer that the catalytically active species are well approximated as $Ir_4$ tetrahedra. Small structural modifications (e.g., an increase in the Ir−Ir bond distance) were observed during catalysis, as described below.

Similar results were observed for hydrogenation of ethene and of propene.[4,14,26,27]

EXAFS structural parameters, including bond distances and coordination numbers, representing $Ir_4/\gamma$-$Al_2O_3$ during catalytic hydrogenation of ethene and of propene are correlated with TOF in Figure 3A−D. Because the conversions were substantially

**TABLE 5: Influence of Co-reactant Partial Pressure on $H_2$ and Hydrocarbon (HC) Reaction Orders for Ethene and Propene Hydrogenation on $\gamma$-$Al_2O_3$-Supported Iridium Clusters**

| catalyst | hydrocarbon (HC) | $T$, K | (range of) $P_{H2}$, Torr | (range of) $P_{HC}$, Torr | reaction order in $H_2$ | reaction order in HC |
|---|---|---|---|---|---|---|
| $Ir_4/\gamma$-$Al_2O_3$ | ethene | 273 | 50−300 | 40 | 0.68 | − |
| $Ir_4/\gamma$-$Al_2O_3$ | ethene | 273 | 100−300 | 100 | 0.9 | − |
| $Ir_4/\gamma$-$Al_2O_3$ | ethene | 273 | 75−300 | 200 | 1.3 | − |
| $Ir_4/\gamma$-$Al_2O_3$ | ethene | 273 | 250−500 | 250 | 0.8 | − |
| $Ir_6/\gamma$-$Al_2O_3$ | ethene | 273 | 50−300 | 40 | 0.6 | − |
| $Ir_6/\gamma$-$Al_2O_3$ | ethene | 273 | 100−300 | 100 | 0.81 | − |
| $Ir_6/\gamma$-$Al_2O_3$ | ethene | 273 | 250−400 | 250 | 0.71 | − |
| $Ir_4/\gamma$-$Al_2O_3$ | propene | 273 | 50−400 | 40 | 0.66 | − |
| $Ir_4/\gamma$-$Al_2O_3$ | propene | 273 | 50−600 | 75 | 0.71 | − |
| $Ir_4/\gamma$-$Al_2O_3$ | propene | 273 | 300−500 | 200 | 0.57 | − |
| $Ir_4/\gamma$-$Al_2O_3$ | propene | 273 | 300−443 | 300 | 0.62 | − |
| $Ir_6/\gamma$-$Al_2O_3$ | ethene | 273 | 100 | 10−200 | − | −0.49 |
| $Ir_6/\gamma$-$Al_2O_3$ | ethene | 273 | 300 | 40−150 | − | −0.18 |
| $Ir_6/\gamma$-$Al_2O_3$ | ethene | 273 | 400 | 250−360 | − | 0.75 |
| $Ir_4/\gamma$-$Al_2O_3$ | propene | 273 | 100 | 10−75 | − | −0.28 |
| $Ir_4/\gamma$-$Al_2O_3$ | propene | 273 | 250 | 200−300 | − | 1.24 |
| $Ir_4/\gamma$-$Al_2O_3$ | propene | 273 | 300 | 100−300 | − | 0.93 |

higher than differential and EXAFS is a sample-averaging technique, the results characterizing $Ir_4/\gamma$-$Al_2O_3$ (and other samples) are interpreted only qualitatively. During the reaction of each alkene, an increase in the Ir−Ir bond distance was observed with increasing TOF; the distance increased more sharply when the reactant was propene than when it was ethene. The Debye−Waller factor characterizing the Ir−Ir contribution decreased with an increasing reaction rate for each alkene. These data indicate that the clusters became more ordered (with less variation in bond distance) with increasing catalyst activity and thereby, presumably, with increasing concentration of reactive adsorbates on the clusters.[4] Similarly, for each alkene there was a decrease in the coordination number characterizing the Ir-support-oxygen bond with increasing TOF, accompanied by an increase in the coordination number characterizing the longer (nonbonding) Ir−O contribution. These data indicate that clusters, while maintaining their bonding to the support during catalysis, underwent slight rearrangements to accommodate cluster-bound reactive intermediates.

*$Ir_4$/MgO.* EXAFS parameters characterizing $Ir_4$/MgO in He at 293 K and 760 Torr (Table 7) are also consistent with the expected tetrahedral $Ir_4$ clusters.[7] EXAFS parameters characterizing $Ir_4$/MgO during toluene hydrogenation catalysis at 760 Torr ($P_{He}$, 118 Torr; $P_{H2}$, 638 Torr; $P_{toluene}$, 4 Torr) and temperatures ranging from 293 to 323 K show that the $Ir_4$ cluster structure was essentially unchanged during reaction (Table 7). (The conversion of toluene ranged from 28 to 86% during these experiments as the temperatures ranged from 293 to 323 K.) Because the tetrahedral $Ir_4$ geometry was maintained during catalysis and the support was catalytically inactive, we infer that $Ir_4$ tetrahedra were the catalytically active species. EXAFS parameters characterizing $Ir_4$/MgO in He at 323 K and 760 Torr following catalysis show that the catalyst slowly returned to its original structure as the reactants were purged from the reactor (Table 7).

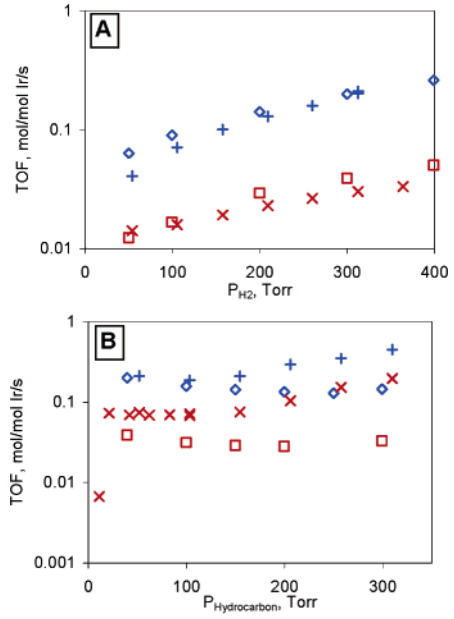


**Figure 1.** (A) Dependence of alkene hydrogenation activity on $H_2$ partial pressure at 273 K and 760 Torr with 40−50 Torr alkene partial pressures. (B) Dependence on alkene partial pressure at 273 K and 760 Torr with 300−310 Torr $H_2$ partial pressures. Symbols: ethene hydrogenation on $Ir_4/\gamma$-$Al_2O_3$ (◊); propene hydrogenation on $Ir_4/\gamma$-$Al_2O_3$ (+); ethene hydrogenation on $Ir_4$/MgO (□); propene hydrogenation on $Ir_4$/MgO (×).

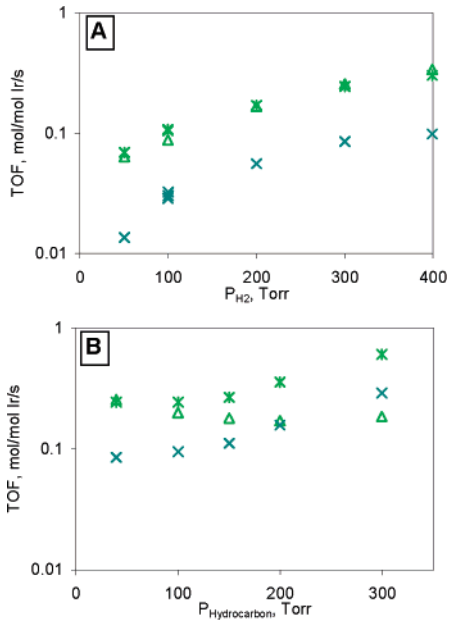


**Figure 2.** (A) Dependence of alkene hydrogenation activity on $H_2$ partial pressure at 273 K and 760 Torr at 40 Torr alkene partial pressure. (B) Dependence of activity on alkene partial pressure at 273 K and 760 Torr at 300 Torr $H_2$ partial pressure. Symbols: ethene hydrogenation on $Ir_{Agg}/\gamma$-$Al_2O_3$ (◊); propene hydrogenation on $Ir_{Agg}/\gamma$-$Al_2O_3$ (∗); propene hydrogenation on $Ir_{Agg}$/MgO (×).

**TABLE 6: EXAFS Fit Parameters Characterizing $\gamma$-$Al_2O_3$-Supported $Ir_4$ Scanned Before and During Toluene Hydrogenation Catalysis at 298 K and 760 Torr[a]**

| | | metal−backscatterer pair | | | | | | | | | | | | | | | |
|---|---|---|---|---|---|---|---|---|---|---|---|---|---|---|---|---|---|
| | | Ir−Ir | | | | Ir−O | | | | Ir−C | | | | Ir−Al | | | |
| atmosphere | $X$[d] | $N$ | $R$, Å | $\Delta\sigma^2 \times 10^3$, Å$^2$ | $\Delta E_0$, eV | $N$ | $R$, Å | $\Delta\sigma^2 \times 10^3$, Å$^2$ | $\Delta E_0$, eV | $N$ | $R$, Å | $\Delta\sigma^2 \times 10^3$, Å$^2$ | $\Delta E_0$, eV | $N$ | $R$, Å | $\Delta\sigma^2 \times 10^3$, Å$^2$ | $\Delta E_0$, eV |
| He[b] | − | 3.2 | 2.65 | 4.5 | 0.0 | 0.3 | 2.14 | −5.0 | −9.3 | 0.3 | 1.94 | −2.7 | −2.0 | 0.9 | 2.73 | −3.8 | 5.7 |
| | | | | | | 0.6 | 3.33 | −2.3 | −2.6 | | | | | 0.4 | 3.63 | −2.6 | 0.4 |
| toluene + $H_2$; catalysis[c] | not measured | 3.2 | 2.69 | 5.1 | −3.7 | 0.2 | 2.13 | −3.0 | −9.7 | − | − | − | − | 1.2 | 2.76 | −2.5 | 4.7 |
| | | | | | | 1.0 | 3.43 | −0.1 | −6.3 | | | | | | | | |

[a] Notation: $N$, coordination number; $R$, absorber-backscatterer distance; $\Delta\sigma^2$, Debye−Waller factor; and $\Delta E_0$, inner potential correction. The approximate experimental uncertainties are as follows: $N$ (±10%), $R$ (±0.02 Å), $\Delta\sigma^2$ (±20%), and $\Delta E_0$ (±20%).[30] [b] Total gas flow rate of 12.4 mL min$^{-1}$. [c] Flow rates of 5 mL min$^{-1}$ He, 11 mL min$^{-1}$ $H_2$, and 0.16 mL min$^{-1}$ $C_7H_8$. [d] $X$, conversion.

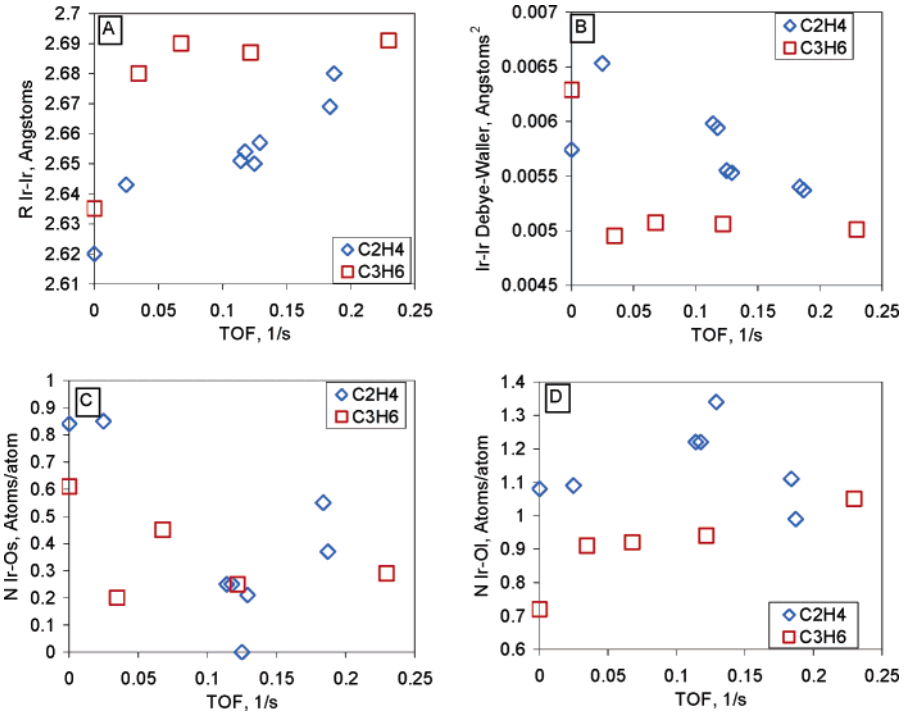


**Figure 3.** EXAFS parameters characterizing $Ir_4/\gamma$-$Al_2O_3$ during ethene hydrogenation catalysis (131−292 Torr of $H_2$, 210−203 Torr of $C_2H_4$, and 253−301 K) and propene hydrogenation catalysis (358 Torr of $H_2$, 134 Torr of $C_3H_6$, and 253−283 K). (A) Ir−Ir bond distance correlated with average catalytic activity (TOF). (B) Ir−Ir Debye−Waller factor correlated with TOF. (C) Ir−$O_{short}$ coordination number correlated with TOF. (D) Ir−$O_{long}$ coordination number correlated with TOF.

EXAFS parameters representing $Ir_4$/MgO during catalytic hydrogenation of ethene, propene, and toluene are plotted against TOF in Figure 4A−D. In each case, the Ir−Ir bond distance increased with increasing TOF. The increase was gradual for ethene, more pronounced for propene, and quite sharp for toluene. The Debye−Waller factor characterizing the Ir−Ir contribution decreased with an increasing rate of the catalytic reaction, with the pattern being similar for the reactions of ethene and propene. In contrast, when the reactant was toluene, the Debye−Waller factor decreased sharply with small increases in TOF.

For each of the hydrocarbon reactants, the coordination number characterizing the metal−support-oxygen bonding decreased with an increasing catalytic reaction rate, with the decrease being sharp for toluene but gradual for ethene and propene. With each of these hydrocarbon reactants, there was an increase in the metal−oxygen coordination number characterizing the nonbonding interaction with increasing TOF, with the increase being sharp for toluene but gradual for propene and even less pronounced for ethene.

*$Ir_6/\gamma$-$Al_2O_3$.* EXAFS parameters characterizing $Ir_6/\gamma$-$Al_2O_3$ in He at 298 K and 760 Torr (Table 8) are consistent with the expected octahedral $Ir_6$ clusters.[8] EXAFS parameters representing $Ir_6/\gamma$-$Al_2O_3$ during toluene hydrogenation at 760 Torr ($P_{He}$, 413 Torr; $P_{H2}$, 334 Torr, $P_{toluene}$, 14 Torr) and temperatures ranging from 299 to 353 K show that the $Ir_6$ cluster structure was essentially unchanged during reaction (Table 8). (In these experiments, the conversion ranged from 18 to 63% and the temperature ranged from 299 to 353 K.) Because the octahedral frame of $Ir_6$ was essentially maintained during catalysis and the support was catalytically inactive, we infer that the catalytically active species are well approximated as $Ir_6$ octahedra. EXAFS parameters characterizing $Ir_6/\gamma$-$Al_2O_3$ in He at 353 K and 760 Torr following catalysis show that the catalyst slowly returned to its original structure as the reactants were purged from the reactor (Table 8).

EXAFS parameters characterizing $Ir_6/\gamma$-$Al_2O_3$ during catalytic hydrogenation of ethene and of toluene are plotted against TOF in Figure 5A−C. In the presence of each hydrocarbon, there

**TABLE 7: EXAFS Fit Parameters Characterizing MgO-Supported $Ir_4$ Scanned during Toluene Hydrogenation Catalysis[a] and in Flowing He[b]**

| | | | metal−backscatterer pair | | | | | | | | | | | | | | | |
|---|---|---|---|---|---|---|---|---|---|---|---|---|---|---|---|---|---|---|
| | | | Ir−Ir | | | | Ir−O | | | | Ir−Mg | | | | Ir−C | | | |
| *T*, K | atmosphere | $X^{c,d}$ | *N* | *R*, Å | $\Delta\sigma^2 \times 10^3$, Å$^2$ | $\Delta E_0$, eV | *N* | *R*, Å | $\Delta\sigma^2 \times 10^3$, Å$^2$ | $\Delta E_0$, eV | *N* | *R*, Å | $\Delta\sigma^2 \times 10^3$, Å$^2$ | $\Delta E_0$, eV | *N* | *R*, Å | $\Delta\sigma^2 \times 10^3$, Å$^2$ | $\Delta E_0$, eV |
| 293 | He | − | 2.9 | 2.62 | 6.8 | 1.1 | 1.1 | 2.05 | −4.4 | 1.0 | 0.6 | 2.45 | 1.5 | 0.7 | 0.5 | 1.91 | −7.9 | −11.2 |
| | | | | | | | 0.5 | 3.33 | −5.2 | −9.0 | | | | | | | | |
| 293 | toluene + $H_2$; catalysis | 0.28 | 3.1 | 2.68 | 5.7 | −1.6 | 0.4 | 2.02 | −4.8 | −1.9 | | | | | 0.6 | 3.28 | −7.3 | −5.4 |
| | | | | | | | 1.0 | 2.63 | −3.7 | 1.4 | | | | | | | | |
| 306 | toluene + $H_2$; catalysis | 0.53 | 3.0 | 2.68 | 4.8 | 0.0 | 0.4 | 1.99 | −4.4 | 0.2 | 0.6 | 2.57 | −1.7 | −3.8 | 0.8 | 3.27 | −7.3 | 0.6 |
| | | | | | | | 1.0 | 2.59 | −4.3 | −4.7 | | | | | | | | |
| 323 | toluene + $H_2$; catalysis | 0.86 | 3.0 | 2.68 | 4.8 | 0.0 | 0.3 | 1.99 | −4.7 | 0.0 | 0.7 | 2.57 | −1.7 | −6.8 | 0.8 | 3.26 | −7.6 | 6.4 |
| | | | | | | | 1.1 | 2.60 | −4.3 | −7.7 | | | | | | | | |
| 323 | He | − | 3.0 | 2.67 | 4.5 | 2.3 | 0.3 | 1.98 | −4.5 | 3.6 | 0.5 | 2.55 | −0.5 | 14.3 | 1.0 | 3.28 | −6.9 | −0.6 |
| | | | | | | | 1.7 | 2.62 | −4.3 | −0.5 | | | | | | | | |

[a] Reaction conditions: 118 Torr He, 638 Torr $H_2$, 4 Torr $C_7H_8$, and temperatures ranging from 293 to 323 K. [b] Same notation as Table 4. [c] *X*, conversion. [d] Total flow rate approximately 46 mL min$^{-1}$.

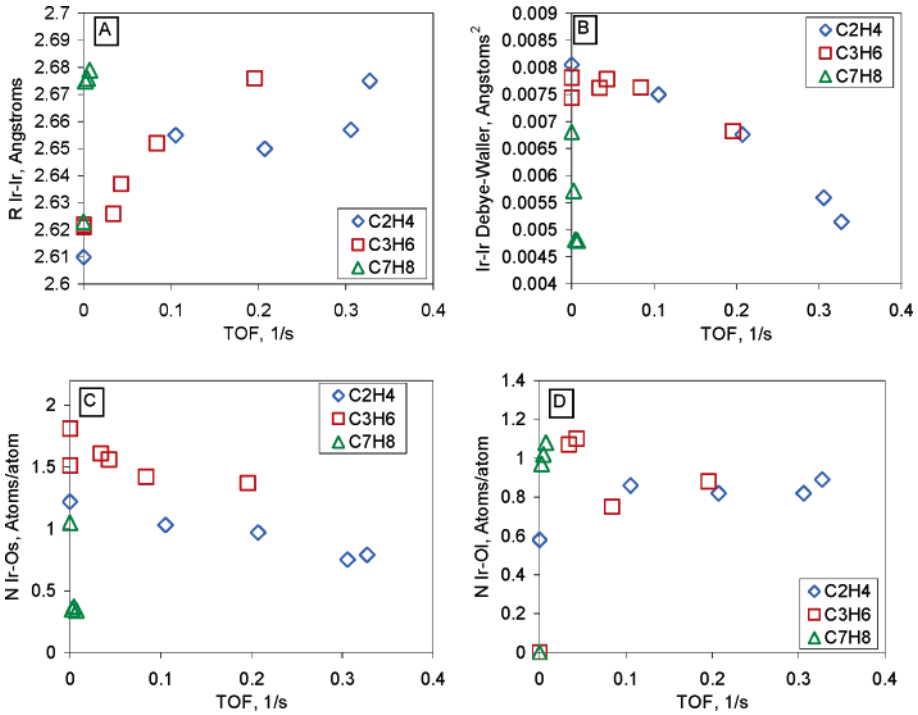


**Figure 4.** EXAFS parameters characterizing $Ir_4$/MgO during ethene hydrogenation catalysis (127−397 Torr of $H_2$, 267−225 Torr of $C_2H_4$, and 298 K), propene hydrogenation catalysis (358 Torr of $H_2$, 134 Torr of $C_3H_6$, and 240−295 K), and toluene hydrogenation (638 Torr of $H_2$, 4 Torr of $C_7H_8$, and 293−323 K). (A) Ir−Ir bond distance correlated with average catalytic activity (TOF). (B) Ir−Ir Debye−Waller factor correlated with TOF. (C) Ir−$O_{short}$ coordination number correlated with TOF. (D) Ir−$O_{long}$ coordination number correlated with TOF.

was an increase in Ir−Ir bond distance with increasing TOF. With each hydrocarbon, there was a decrease in the Debye−Waller factor characterizing the Ir−Ir contribution, with the decrease being more pronounced for the reaction of toluene than that of ethene. In each case, there was a decrease in the coordination number of the Ir−O bonding contribution with increasing reaction rate. The decrease was most pronounced for ethene, and for toluene, the Ir−O bonding contribution became negligibly small (e.g., less than 0.3 on average) upon commencement of the catalytic reaction.

*$Ir_6$/MgO.* EXAFS parameters characterizing $Ir_6$/MgO in He at 301 K and 760 Torr (Table 9) are consistent with the expected octahedral $Ir_6$ clusters.[11] EXAFS parameters characterizing $Ir_6$/MgO during toluene hydrogenation catalysis at 760 Torr ($P_{He}$, 413 Torr; $P_{H2}$, 334 Torr; $P_{toluene}$, 14 Torr) and temperatures ranging from 299 to 358 K show that the $Ir_6$ cluster structure was essentially unchanged during reaction (Table 9). (The toluene conversion ranged from 3 to 38% and the temperature from 299 to 358 K in these experiments.) Because the $Ir_6$ octahedral geometry was maintained during catalysis and the support was catalytically inactive, we infer that the catalytically active species are well approximated as $Ir_6$ octahedra. EXAFS parameters characterizing $Ir_6$/MgO in He at 210 K and 760 Torr following catalysis again show that the catalyst slowly returned to its original structure as the reactants were purged from the reactor (Table 9).

EXAFS parameters characterizing $Ir_6$/MgO during hydrogenation of ethene and of toluene are plotted against TOF in Figure

**TABLE 8: EXAFS Fit Parameters Characterizing $\gamma$-$Al_2O_3$-Supported $Ir_6$ Scanned during Toluene Hydrogenation Catalysis[a] and in Flowing He[b]**

| | | | metal−backscatterer pair | | | | | | | | | | | | | | | |
|---|---|---|---|---|---|---|---|---|---|---|---|---|---|---|---|---|---|---|
| | | | Ir−Ir | | | | Ir−O | | | | Ir−C | | | | Ir−Al | | | |
| *T*, K | atmosphere | $X^{c,d}$ | *N* | *R*, Å | $\Delta\sigma^2 \times 10^3$, Å$^2$ | $\Delta E_0$, eV | *N* | *R*, Å | $\Delta\sigma^2 \times 10^3$, Å$^2$ | $\Delta E_0$, eV | *N* | *R*, Å | $\Delta\sigma^2 \times 10^3$, Å$^2$ | $\Delta E_0$, eV | *N* | *R*, Å | $\Delta\sigma^2 \times 10^3$, Å$^2$ | $\Delta E_0$, eV |
| 293 | He | − | 4.3 | 2.62 | 7.7 | 0.0 | 1.3 | 2.04 | 2.9 | 2.2 | 0.3 | 1.84 | −4.2 | 3.1 | 0.2 | 3.10 | −3.8 | 0.0 |
| | | | 1.3 | 3.74 | 9.1 | 0.0 | 1.0 | 2.75 | 8.6 | −14.3 | | | | | | | | |
| 299 | toluene + $H_2$; catalysis | 0.18 | 4.1 | 2.66 | 5.9 | 0.0 | 1.2 | 2.66 | −2.2 | −9.4 | 0.5 | 2.00 | −1.5 | 2.5 | 0.4 | 3.11 | −2.3 | −3.4 |
| | | | 1.2 | 3.76 | 4.9 | 0.0 | | | | | | | | | | | | |
| 314 | toluene + $H_2$; catalysis | 0.25 | 3.9 | 2.66 | 5.4 | 0.0 | 1.1 | 2.65 | −2.8 | − | 0.4 | 2.00 | −1.7 | −1.2 | 0.4 | 3.10 | 0.6 | −5.4 |
| | | | 1.6 | 3.75 | 5.9 | 0.0 | 10.5 | | | | | | | | | | | |
| | | | | | | | 0.6 | 3.48 | −3.4 | −0.3 | | | | | | | | |
| 343 | toluene + $H_2$; catalysis | 0.54 | 3.9 | 2.66 | 5.7 | 0.0 | 1.4 | 2.66 | -2.4 | -9.2 | 0.4 | 1.97 | -0.7 | 3.3 | 0.3 | 3.09 | -3.2 | -0.2 |
| | | | 1.4 | 3.77 | 5.0 | 0.0 | 0.6 | 3.49 | -4.3 | -3.0 | | | | | | | | |
| 353 | toluene + $H_2$; catalysis | 0.63 | 3.9 | 2.66 | 5.5 | 0.0 | 1.4 | 2.66 | −2.4 | −10.7 | 0.5 | 1.98 | −0.7 | 3.3 | 0.5 | 3.10 | 0.7 | −0.52 |
| | | | 1.4 | 3.77 | 5.6 | 0.0 | 0.4 | 3.49 | −4.3 | 1.8 | | | | | | | | |
| 353 | He | − | 3.9 | 2.65 | 6.4 | 0.0 | 1.4 | 2.66 | −3.1 | −10.4 | 0.4 | 1.99 | −4.4 | 4.3 | 0.5 | 3.10 | −3.2 | −5.4 |
| | | | 1.2 | 3.75 | 3.6 | 0.0 | 0.7 | 3.38 | −3.8 | 13.9 | | | | | | | | |

[a] Reaction conditions: 413 Torr He, 334 Torr $H_2$, 14 Torr $C_7H_8$, and temperatures ranging from 299 to 353 K. [b] Same notation as Table 4. [c] *X*, conversion. [d] Total flow rate approximately 52 mL min$^{-1}$.

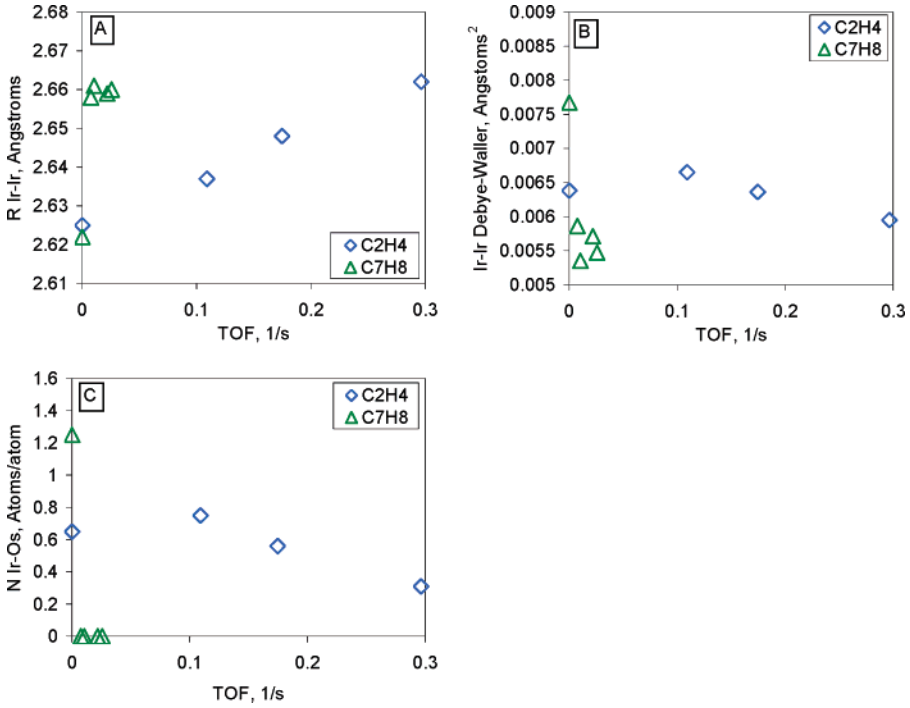


**Figure 5.** EXAFS parameters characterizing $Ir_6/\gamma$-$Al_2O_3$ during ethene hydrogenation catalysis (127−397 Torr of $H_2$, 267−225 Torr of $C_2H_4$, and 298 K) and toluene hydrogenation catalysis (334 Torr of $H_2$, 14 Torr of $C_7H_8$, and 299−353 K). (A) Ir−Ir bond distance (1st shell) correlated with average catalytic activity (TOF). (B) Ir−Ir Debye−Waller factor (1st shell) correlated with TOF. (C) Ir−$O_{short}$ coordination number correlated with TOF.

6A−D. Again, with each hydrocarbon, there was an increase in the Ir−Ir bond distance with increasing TOF. The patterns in the data are similar to those stated above for the other reactants.

*$Rh_6$/MgO*. EXAFS parameters characterizing $Rh_6$/MgO in He at 299 K and 760 Torr (Table 10) are consistent with the expected octahedral $Rh_6$ clusters.[12] EXAFS parameters characterizing $Rh_6$/MgO during toluene hydrogenation at 760 Torr ($P_{He}$, 413 Torr; $P_{H2}$, 334 Torr; $P_{toluene}$, 14 Torr) and temperatures ranging from 299 to 339 K show that the $Rh_6$ cluster structure was essentially unchanged during reaction (Table 10). (The toluene conversion ranged from 11 to 38% in these experiments, and the temperature ranged from 299 to 338 K.) Because the $Rh_6$ octahedral geometry was maintained during catalysis and the support was catalytically inactive, we infer that the catalytically active species are well approximated as $Rh_6$ octahedra. Again, small structural modifications were observed during catalysis, and EXAFS parameters characterizing $Rh_6$/MgO in He at 338 K and 760 Torr following catalysis show that the catalyst slowly returned to its original structure as the reactants were purged from the reactor (Table 10).

EXAFS parameters characterizing $Rh_6$/MgO during hydrogenation of ethene and of toluene are plotted against TOF in Figure 7A−D. The Rh−Rh bond distance increased with an

**TABLE 9: EXAFS Fit Parameters Characterizing MgO-Supported $Ir_6$ Scanned during Toluene Hydrogenation Catalysis[a] and in Flowing He[b]**

| | | | metal−backscatterer pair | | | | | | | | | | | | | | | |
|---|---|---|---|---|---|---|---|---|---|---|---|---|---|---|---|---|---|---|
| | | | Ir−Ir | | | | Ir−O | | | | Ir−C | | | | Ir−Mg | | | |
| *T*, K | atmosphere | $X$[c,d] | *N* | *R*, Å | $\Delta\sigma^2 \times 10^3$, Å$^2$ | $\Delta E_0$, eV | *N* | *R*, Å | $\Delta\sigma^2 \times 10^3$, Å$^2$ | $\Delta E_0$, eV | *N* | *R*, Å | $\Delta\sigma^2 \times 10^3$, Å$^2$ | $\Delta E_0$, eV | *N* | *R*, Å | $\Delta\sigma^2 \times 10^3$, Å$^2$ | $\Delta E_0$, eV |
| 301 | He | − | 3.9 | 2.61 | 9.4 | 0.0 | 1.1 | 2.02 | 2.1 | 2.0 | − | − | − | − | 0.4 | 2.91 | −4.6 | 12.7 |
| | | | 1.0 | 3.80 | 5.9 | −2.0 | 0.5 | 3.30 | −0.5 | −8.4 | | | | | | | | |
| 299 | toluene + $H_2$; catalysis | 0.03 | 3.9 | 2.66 | 5.9 | −1.0 | 0.4 | 2.07 | −5.3 | 1.6 | 0.4 | 1.90 | −7.0 | 11.2 | 0.5 | 3.05 | −1.3 | 13.2 |
| | | | | | | | 0.6 | 2.59 | −0.8 | 12.2 | | | | | | | | |
| | | | | | | | 0.9 | 3.28 | −4.8 | 2.9 | | | | | | | | |
| 319 | toluene + $H_2$; catalysis | 0.12 | 4.0 | 2.68 | 6.1 | 0.0 | 0.4 | 2.02 | −3.0 | 4.5 | 0.2 | 1.87 | −7.0 | − | 0.8 | 3.06 | 2.8 | 7.9 |
| | | | | | | | 1.0 | 2.64 | −3.2 | −7.5 | 11.9 | | | | | | | |
| 338 | toluene + $H_2$; catalysis | 0.27 | 4.0 | 2.68 | 6.0 | −2.3 | 0.7 | 2.65 | −2.9 | −2.0 | 0.3 | 1.87 | −5.9 | 8.8 | 0.3 | 3.22 | −1.0 | 15.5 |
| | | | 1.0 | 3.78 | 6.8 | 3.1 | | | | | | | | | | | | |
| 358 | toluene + $H_2$; catalysis | 0.38 | 4.0 | 2.68 | 5.6 | 0.0 | 0.4 | 2.04 | −3.9 | 0.9 | 0.3 | 1.88 | −7.0 | −7.0 | 1.0 | 3.03 | 4.1 | 13.2 |
| | | | | | | | 1.3 | 2.67 | −3.2 | −9.7 | | | | | | | | |
| 210 | He | − | 3.9 | 2.65 | 6.3 | 1.2 | 0.6 | 2.04 | −3.2 | 2.7 | 0.3 | 1.89 | −7.6 | −6.5 | − | − | − | − |
| | | | | | | | 1.0 | 2.55 | 1.4 | 5.9 | | | | | | | | |
| | | | | | | | 0.7 | 3.33 | −3.9 | −4.4 | | | | | | | | |

[a] Reaction conditions: 413 Torr He, 334 Torr $H_2$, 14 Torr $C_7H_8$, and temperatures ranging from 299 to 353 K. [b] Same notation as Table 4. [c] $X$, conversion. [d] Total flow rate approximately 52 mL min$^{-1}$.

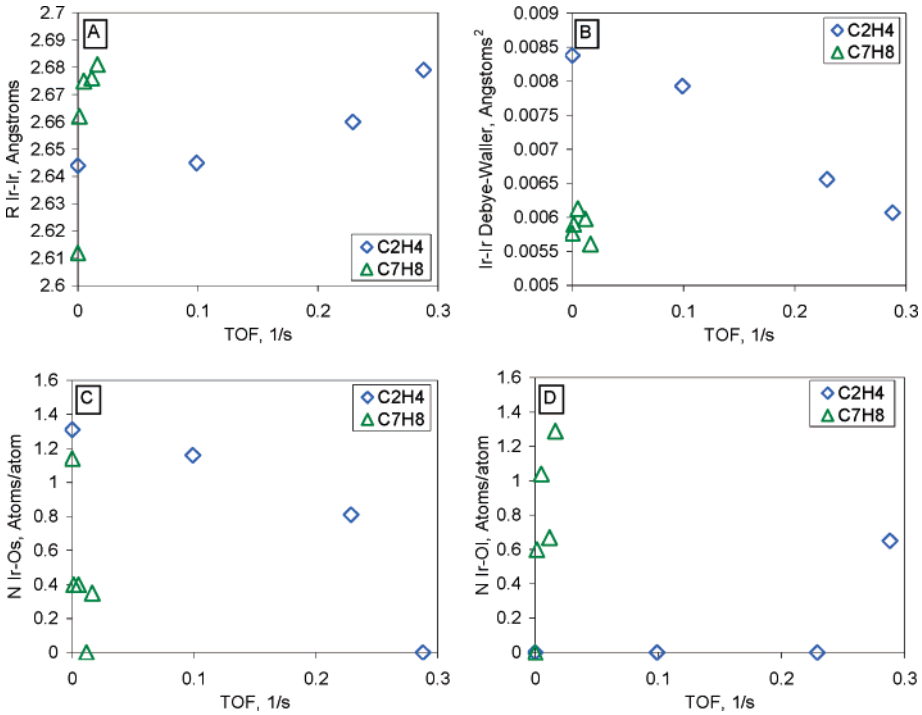


**Figure 6.** EXAFS parameters characterizing $Ir_6$/MgO during ethene hydrogenation catalysis (127−277 Torr of $H_2$, 267−243 Torr of $C_2H_4$, and 298 K) and toluene hydrogenation catalysis (334 Torr of $H_2$, 14 Torr of $C_7H_8$, and 299−358 K). (A) Ir−Ir bond distance (1st shell) correlated with average catalytic activity (TOF). (B) Ir−Ir Debye−Waller (1st shell) correlated with TOF. (C) Ir−$O_{short}$ coordination number correlated with TOF. (D) Ir−$O_{long}$ coordination number correlated with TOF.

increasing reaction rate when the reactant hydrocarbon was ethene, but there was no noticeable effect when the reactant was toluene. With each hydrocarbon, there was a decrease in the Debye−Waller factor characterizing the Rh−Rh contribution with increasing reaction rate, accompanied by a decrease in the coordination number characterizing the Rh−O bonding and an increase in the coordination number characterizing the nonbonding Rh−O contribution.

## Discussion

**Hydrogenation of Alkenes and of Toluene on Supported Metal Clusters.** *Hydrogenation of Alkenes.* IR spectra of the

**TABLE 10: EXAFS Fit Parameters Characterizing MgO-Supported $Rh_6$ Scanned during Toluene Hydrogenation Catalysis[a] and in Flowing He[b]**

| | | | metal−backscatterer pair | | | | | | | | | | | | | | | |
|---|---|---|---|---|---|---|---|---|---|---|---|---|---|---|---|---|---|---|
| | | | Rh−Rh | | | | Rh−O | | | | Rh−C | | | | Rh−Mg | | | |
| *T*, K | atmosphere | *X*[c,d] | *N* | *R*, Å | $\Delta\sigma^2 \times 10^3$, Å$^2$ | $\Delta E_0$, eV | *N* | *R*, Å | $\Delta\sigma^2 \times 10^3$, Å$^2$ | $\Delta E_0$, eV | *N* | *R*, Å | $\Delta\sigma^2 \times 10^3$, Å$^2$ | $\Delta E_0$, eV | *N* | *R*, Å | $\Delta\sigma^2 \times 10^3$, Å$^2$ | $\Delta E_0$, eV |
| 299 | He | − | 4.2 | 2.66 | 7.4 | 4.1 | 0.6 | 2.18 | 3.0 | −13.0 | 0.2 | 2.03 | −3.8 | −4.2 | 0.7 | 3.22 | 1.2 | −14.0 |
| | | | 1.4 | 3.63 | 10.4 | 10.7 | | | | | | | | | | | | |
| 299 | toluene + $H_2$; catalysis | 0.11 | 4.0 | 2.66 | 6.3 | 6.4 | 0.3 | 2.10 | −6.1 | 10.8 | 0.3 | 2.00 | −1.8 | 3.6 | 0.4 | 3.30 | −1.1 | −10.2 |
| | | | 1.4 | 3.63 | 10.1 | 11.6 | 0.9 | 2.67 | −5.4 | −2.5 | | | | | | | | |
| 313 | toluene + $H_2$; catalysis | 0.25 | 4.0 | 2.66 | 6.5 | 6.9 | 0.3 | 2.11 | −4.0 | −2.5 | 0.3 | 2.00 | −2.3 | −0.2 | 0.6 | 3.10 | 1.3 | 0.6 |
| | | | 1.4 | 3.63 | 14.8 | 9.2 | 0.7 | 2.69 | −5.4 | 4.5 | | | | | | | | |
| 328 | toluene + $H_2$; catalysis | 0.35 | 4.2 | 2.65 | 6.9 | 7.4 | 0.4 | 2.09 | −5.9 | 2.9 | 0.3 | 2.01 | −4.6 | −10.0 | 0.6 | 3.19 | 2.6 | −5.0 |
| | | | 1.1 | 3.62 | 13.2 | 10.8 | 0.7 | 2.65 | −5.4 | 1.6 | | | | | | | | |
| 339 | toluene + $H_2$; catalysis | 0.38 | 4.4 | 2.66 | 6.5 | 8.0 | 0.4 | 2.08 | −7.7 | −2.2 | 0.3 | 2.00 | −6.9 | −15.2 | 0.7 | 3.20 | 3.4 | −7.5 |
| | | | 1.6 | 3.63 | 11.7 | 12.7 | 0.7 | 2.67 | −3.9 | 5.7 | | | | | | | | |
| 338 | He | − | 4.0 | 2.66 | 6.9 | 6.5 | 0.4 | 2.09 | −3.9 | −0.9 | 0.2 | 1.98 | −3.8 | −7.1 | 0.7 | 3.26 | 0.1 | −12.5 |
| | | | 0.9 | 3.61 | 5.2 | 13.8 | 0.5 | 2.69 | −5.7 | 2.0 | | | | | | | | |

[a] Reaction conditions: 413 Torr He, 334 Torr $H_2$, 14 Torr $C_7H_8$, and temperatures ranging from 299 to 353 K. [b] Same notation as Table 4. [c] *X*, conversion. [d] Total flow rate of about 52 mL min$^{-1}$.

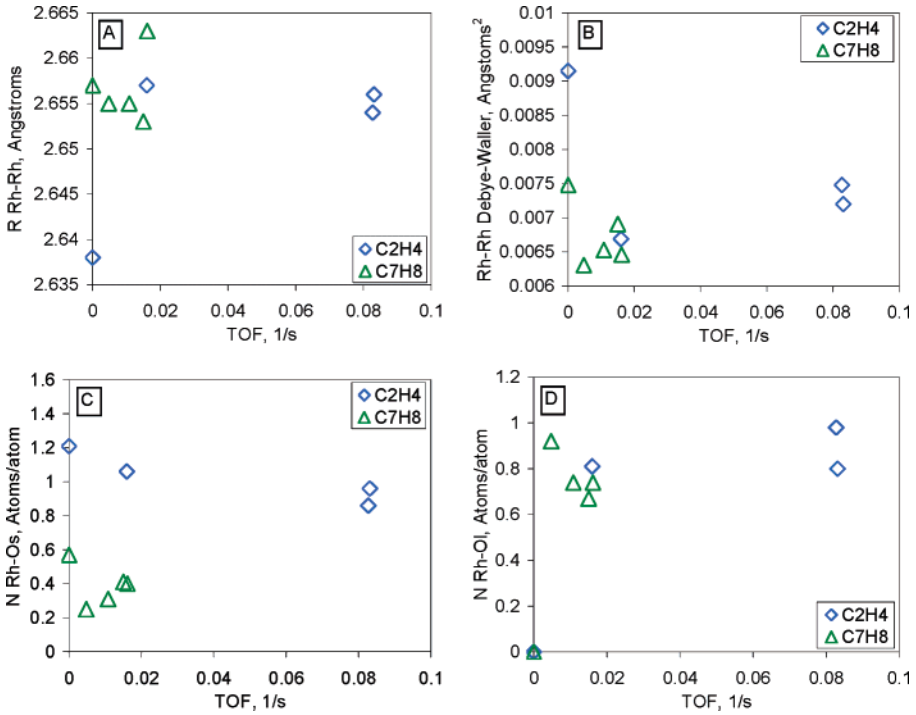


**Figure 7.** EXAFS parameters characterizing $Rh_6$/MgO during ethene hydrogenation catalysis (180 Torr of $H_2$, 209 Torr of $C_2H_4$, and 273−338 K) and toluene hydrogenation catalysis (334 Torr of $H_2$, 14 Torr of $C_7H_8$, and 299−338 K). (A) Rh−Rh bond distance (1st shell) correlated with average catalytic activity (TOF). (B) Rh−Rh Debye−Waller factor (1st shell) correlated with TOF. (C) Rh−$O_{short}$ coordination number correlated with TOF. (D) Rh−$O_{long}$ coordination number correlated with TOF.

functioning alkene hydrogenation catalysts indicate the presence of various hydrocarbon ligands on the metal clusters, formed from the alkene and $H_2$,[4,12,26,27] implying competitive adsorption of the hydrocarbons and hydrogen, consistent with the observed orders of reaction. Dumesic's group,[28−30] investigating $SiO_2$-supported particles of Pt, showed that ethene hydrogenation proceeded via associative adsorption of ethene and dissociative adsorption of $H_2$, followed by stepwise hydrogenation to ethyl and to ethane. Ethene and $H_2$ were found to compete for adsorption sites at high temperatures (and low ethene coverage); however, at low temperatures (or high ethene coverage), ethene was found to adsorb preferentially on the catalyst, forcing $H_2$ to adsorb on sites unavailable to ethene (e.g., edges of metal particles). This representation gives rise to a reaction order in $H_2$ of 0.5−1.0 and a reaction order in ethene that is slightly negative to zero.

The data presented here and in earlier work[4,12,14,26,27] for alkene hydrogenation on supported metal clusters are consistent with the representation proposed by Dumesic and with the general expectation that alkenes adsorb more strongly than $H_2$ on transition metals.[33] Negative alkene reaction orders suggest self-inhibition by strong adsorption; zero order suggests saturation of the catalyst with adsorbates; positive orders suggest lower coverages with adsorbates, with the implication that sites are

available for competitive adsorption of co-reactants. In alkene hydrogenation on oxide-supported rhodium or iridium clusters, the reaction order in alkene is approximately −0.1 to −0.5 at low alkene partial pressures, approximately zero at intermediate alkene partial pressure (identified as the pivotal partial pressure $P_p$), and approximately unity at alkene partial pressures exceeding $P_p$. To repeat, our data show that $P_p$ is approximately 150−200 Torr for ethene hydrogenation and 75−100 Torr for propene hydrogenation.

In catalysis on extended metal surfaces (e.g., single crystals or conventional supported metal particles), the orders of reaction in $H_2$ are usually near 0.5 for low-temperature reactions, indicating equilibrated, noncompetitive $H_2$ adsorption, resulting from the catalyst's being saturated with alkene adsorbates (forcing $H_2$ to adsorb on sites unavailable to alkene).[28−30] As the reaction temperature increases, the reaction order in $H_2$ increases to 1.0 or slightly higher values (1.2−1.3), indicating lower alkene coverage and competitive adsorption of $H_2$. The reaction orders in $H_2$ for alkene hydrogenation on iridium and on rhodium clusters suggest that the alkene is more strongly adsorbed on iridium than on rhodium,[33−35] resulting in more competitive $H_2$ adsorption on rhodium.

If there were significant effects on the rates of the catalytic reactions of adsorption of the reactants on the supports, one would expect the support effects to be greater for the supported clusters than for the larger supported particles (because of the greater metal support interfaces in the former). The data indicate the following ratios of catalytic activities under comparable conditions for $\gamma$-$Al_2O_3$- and MgO-supported $Ir_4$: 5.4 for ethene hydrogenation, 2.3 for propene hydrogenation, and 1.6 for toluene hydrogenation; for $\gamma$-$Al_2O_3$- and MgO-supported $Ir_6$, the ratios are 1.9 for ethene hydrogenation and 7.4 for toluene hydrogenation; and for $\gamma$-$Al_2O_3$- and MgO-supported iridium aggregates, the ratios are 5.9 for ethene hydrogenation and 5.0 for toluene hydrogenation. Thus, these data give no indication of significant effects of adsorption of reactants on the supports.

Previously, we reported IR spectra showing that di-$\sigma$-bonded ethene and ethyl are present (and likely intermediates) in ethane hydrogenation on $Ir_4/\gamma$-$Al_2O_3$ at alkene partial pressures $< P_p$, and $\pi$-bonded ethene and ethyl are likely intermediates in ethene hydrogenation on $Ir_4/\gamma$-$Al_2O_3$ and on $Ir_6/\gamma$-$Al_2O_3$ at alkene partial pressures $> P_p$.[4,27] Similarly, we showed that $\pi$-bonded propene and 1-propyl are intermediates in propene hydrogenation on $Ir_4/\gamma$-$Al_2O_3$ and on $Ir_4$/MgO at propene partial pressures $> P_p$.[4,14]

Using first-principles calculations, Neurock and van Santen[32] demonstrated that repulsive adsorbate−adsorbate interactions lower the energy barrier for hydrogenation via $\pi$-bonded ethene, whereas in the absence of these interactions (i.e., at low coverages), hydrogenation is energetically favored to proceed via di-$\sigma$-bonded ethene. (Adsorbate−adsorbate interactions on the surface of Pd(111) significantly reduce the strength of Pd−H and Pd−C bonds, making direct hydrogenation from $\pi$-bonded ethene, via a "slip" mechanism,[36] energetically favorable.)

IR data recorded during alkene hydrogenation on supported metal cluster catalysts[4,27] point to a shift in the reaction mechanism at $P_p$: for $P_{alkene} < P_p$, alkene hydrogenation proceeds predominantly via di-$\sigma$-bonded alkene (to an alkyl intermediate and then to the alkane), whereas for $P_{alkene} > P_p$, hydrogenation initially proceeds via $\pi$-bonded alkene. We suggest that this mechanistic shift may be attributed to increased adsorbate−adsorbate interactions on the clusters at higher hydrocarbon coverages.[27]

As the interaction of the clusters with the support affects the bonding of the clusters to reactive intermediates, the bonding of reactive intermediates to the clusters likewise affects the cluster structure and its bonding to the support. Earlier we showed that as the concentration of reactive intermediates on $Ir_4$ increased (accompanied by an increase in the catalytic reaction rate), the metal−metal bond distance in the clusters increased as well;[4] furthermore, part of the metal−short oxygen coordination shell, indicating bonding of the clusters to the support, was replaced by a longer nonbonding metal−oxygen shell (with a distance of approximately 2.6 Å). These results indicate that, during catalysis, the clusters flex away from the support as bonds are created with reactive intermediates (this is a modification of the ligand environment of the cluster). Similar types of structural modifications were observed during toluene hydrogenation on supported metal clusters (Tables 6−10) with EXAFS spectroscopy.

*Differences Between Alkene and Arene Hydrogenation.* Hydrogenation of ethene proceeds similarly to hydrogenation of propene, either on clusters or extended metal surfaces, but the hydrogenation of toluene on these materials proceeds quite differently. Whereas ethene- and propene-derived adsorbates are identifiable by IR spectroscopy during catalysis, the number of intermediates and the complexity of the toluene-derived adsorbates render IR spectroscopy an ineffective technique for investigating intermediates in toluene hydrogenation on supported metal clusters. The rates of toluene hydrogenation are an order of magnitude lower than those of alkenes, even at temperatures 60 K higher (Table 1). The reaction order in $H_2$ is approximately unity for toluene hydrogenation, but only 0.6−0.8 for alkene hydrogenation, indicating that $H_2$ adsorbs in a competitive fashion in toluene hydrogenation and in either competitive or noncompetitive fashion in alkene hydrogenation (Table 3). The results indicate that $H_2$ is able to adsorb on sites unavailable to alkenes during alkene hydrogenation, whereas toluene adsorption appears to successfully block these "hydrogen-only" sites during toluene hydrogenation.

The hydrocarbon reaction orders differ substantially for toluene hydrogenation and alkene hydrogenation. The reaction order in toluene is approximately constant at 0.1 for toluene partial pressures as low as 10 Torr, whereas the reaction order in alkene is negative for $P_{alkene} < P_p$ and positive for $P_{alkene} > P_p$. This latter point indicates that toluene coverage is substantially more complete than that of alkenes and that adsorbate−adsorbate interactions are less important in toluene hydrogenation than in ethene and propene hydrogenation. Although the data presented here do not definitively identify the source of this difference, we speculate, consistent with the observed activation energies, that toluene-derived adsorbates are bound more strongly to the catalysts, limiting the importance of adsorbate−adsorbate interactions (but we cannot rule out geometric effects).

In addition to large differences in catalytic rates between hydrogenation of toluene and hydrogenation of alkenes, the influence that each type of reactant has on the structure of the clusters during hydrogenation is also different. As in alkene hydrogenation catalysis, the cluster metal−metal bond distance increases and the bonding of the cluster to the support decreases during toluene hydrogenation catalysis. However, these structural modifications occur at much lower catalytic activities and at much lower hydrocarbon partial pressures for toluene hydrogenation than for alkene hydrogenation (for example, similar structural changes are observed for $Ir_4$/MgO in ethene hydrogenation at 225 Torr of ethene and at a TOF of 0.33 $s^{-1}$

compared to values for toluene hydrogenation of 4 Torr of toluene and a TOF of 0.0072 $s^{-1}$). The result is consistent with our postulate stated above that toluene-derived adsorbates bond more strongly to the clusters than do ethene- or propene-derived adsorbates. However, one would expect that toluene has a greater sticking efficiency on metals than alkenes; thus, the data presented here do not allow us to discern whether an increased adsorbate bonding strength or an increased coverage (even at lower partial pressures) results in the greater influence of toluene-derived adsorbates than of ethene- or propene-derived adsorbates on the cluster structure. These two effects have not been separated in the current work given that they both increase going from ethene to toluene.

**Hydrogenation of Ethene and Hydrogenation of Propene on Supported Metal Clusters.** *Similarities in Ethene and Propene Hydrogenation.* Ethene hydrogenation and propene hydrogenation display similar kinetics when catalyzed by supported metal clusters: apparent activation energies ranging from 24 to 40 kJ/mol, reaction orders in $H_2$ of 0.5−1.0, reaction orders in alkene that are slightly negative when $P_{alkene} < P_p$, reaction orders in alkene that are zero when $P_{alkene} \approx P_p$, and reaction orders in alkene near 1 when $P_{alkene} > P_p$.

Thus, it was concluded[12,14,26,27] that ethene hydrogenation and propene hydrogenation proceed by similar mechanisms on supported iridium clusters and rhodium clusters. At low alkene partial pressures, di-$\sigma$-bonded ethene and ethyl (and 1-propyl) have been identified as reaction intermediates for ethene (and propene) hydrogenation. Similarly, at high alkene partial pressures, $\pi$-bonded ethene and ethyl (and $\pi$-bonded propene and 1-propyl) have been identified as reactive intermediates for ethene (and propene) hydrogenation. Ethylidyne and propylidyne have been observed during hydrogenation of the respective alkenes, and they are believed to be essentially spectators (or inhibitors[14]), a pattern that is largely consistent with results characterizing alkene hydrogenation catalysis by single crystals of metal.[37,38]

Furthermore, the presence of cluster-bound reactive intermediates modifies the cluster structure and its attachment to the support similarly for ethene hydrogenation and for propene hydrogenation. Specifically, as the concentration of reactive intermediates on the clusters increases, (a) the cluster frame swells and (b) the clusters flex away from the support (as indicated by an increased M−O bond length and by the conversion of some of the shorter M−O bonding contributions (at approximately 2.1 Å) to longer, nonbonding M−O contributions (at approximately 2.7 Å)).

*Differences between Ethene and Propene Hydrogenation.* Although ethene hydrogenation and propene hydrogenation on supported iridium and rhodium clusters display many qualitative similarities, the two reactions also display some notable differences. Independent of catalyst composition, the alkene partial pressure at which the reaction order in alkene changes from slightly negative to positive is related to the alkene: for ethene hydrogenation, $P_p$ is approximately 150−200 Torr of ethene, whereas for propene hydrogenation, $P_p$ is approximately 75 Torr of propene. As demonstrated by the data in Tables 3 and 5, the reaction orders in $H_2$ are generally lower for propene hydrogenation than for ethene hydrogenation, indicating that $H_2$ is more successful in the competition with alkene for adsorption on the catalyst in ethene hydrogenation and is more restricted to sites unavailable to the hydrocarbon in propene hydrogenation. It is significant, we infer, that at relatively high temperatures or low alkene partial pressures, when coverages of the metal by reactants are relatively low, the rates of hydrogenation and the orders of reaction in $H_2$ become quite similar for the two reactions. Therefore, it appears that the differences between ethene hydrogenation and propene hydrogenation arise primarily from different adsorbate−adsorbate interactions: specifically, adsorbate−adsorbate interactions become significant at lower alkene coverages for propene than for ethene, because it is heavier and larger than ethene.

The IR spectra also indicate subtle differences between hydrogenation of ethene and hydrogenation of propene on supported metal clusters. Whereas alkyl ligands (ethyl or 1-propyl) are observed for the hydrogenation of both alkenes, di-$\sigma$-bonded alkene is observed only for ethene, suggesting different reactivities of the different types of intermediates for the two reactions. Furthermore, ethylidyne was observed only in very low concentrations during ethene hydrogenation, whereas propylidyne was observed in relatively high concentration during propene hydrogenation. Although we have not demonstrated the stability of ethylidyne on the clusters as we have for propylidyne,[26] we might infer on the basis of the stability of ethylidyne on extended metal surfaces[35,39,40] that ethylidyne would be quite stable on the clusters; this reasoning leads to the suggestion that ethylidyne formation is less facile than propylidyne formation under conditions of the respective hydrogenation reactions. Thus, although the data do not completely illuminate the reasons why the different types of adsorbates form to different extents during ethene and propene hydrogenation, they highlight distinct differences between the reactions of the two alkenes and provide hypotheses that might be tested theoretically.

**Differences in Hydrogenation on Clusters and on Particles of Metal.** The data also indicate differences between hydrogenation of alkenes and of arenes on the small metal clusters relative to hydrogenation on the larger metal aggregates. The generalizations are limited, because they are based on comparisons of rates under only one (approximate) set of reaction conditions and because the effects of supports are not fully deconvoluted. The most obvious difference is in the rates of hydrogenation (Table 1); hydrogenation of toluene is slower (typically by an order of magnitude) than hydrogenation of alkenes on the aggregates and 2 orders of magnitude slower on iridium clusters (Table 1). However, this statement does not extend to $Rh_6$ clusters, on which toluene hydrogenation rates are approximately 1 order of magnitude less than ethene hydrogenation rates (Table 1).

The difference between rhodium and iridium is associated with the different apparent activation energies: that for toluene hydrogenation on iridium clusters or aggregates is approximately 50−60 kJ/mol, compared with one of only approximately 30−40 kJ/mol for reaction on the rhodium (Table 2). We suggest that part of the difference, as stated above, is that toluene blocks $H_2$ adsorption more successfully on clusters (corresponding to the slightly positive reaction order in toluene and $H_2$ reaction orders between 0.5 and 1.0) than on extended metal surfaces. Correspondingly, toluene hydrogenation on extended metal surfaces is typically an order of magnitude faster than that on the small clusters. The rhodium clusters are not affected by this suppression of the rate of catalysis to the same extent as iridium clusters, in part, we infer, because the strength of toluene adsorption is substantially less on rhodium than that on iridium.

**Acknowledgment.** This research was supported by the National Science Foundation (AMA, Grant CTS-9617257) and by the U.S. Department of Energy (DOE) (J.F.G., F.S.L., and B.C.G., Grants FG02-87ER13790 and FG02-04ER15513). We acknowledge beam time and the support of the DOE, Division

of Materials Sciences, under Contract No. DE-FG05-89ER45384, for its role in the operation and development of beamline X-11A at the National Synchrotron Light Source, which is supported by the DOE, Division of Materials Sciences and Division of Chemical Sciences, under Contract No. DE-AC02-76CH00016. We are grateful to the staff of beam line X-11A for their assistance. The EXAFS data were analyzed with the software XDAP.[41]

**Supporting Information Available:** Crystallographic data characterizing the reference compounds, EXAFS data, and details of the EXAFS analysis. This material is available free of charge via the Internet at http://pubs.acs.org.

## References and Notes

(1) Avery, N. R.; Sheppard, N. *Proc. R. Soc. London, Ser. A* **1986**, *405*, 1.
(2) Nieuwenhuys, B. E.; Hagen, D. I.; Rovida, G.; Somorjai, G. A. *Surf. Sci.* **1976**, *59*, 155.
(3) Lin, S. D.; Vannice, M. A. *J. Catal.* **1993**, *143*, 563.
(4) Argo, A. M.; Odzak, J. F.; Lai, F. S.; Gates, B. C. *Nature* **2002**, *415*, 623.
(5) Xu, Z.; Xiao, F.-S.; Purnell, S. K.; Alexeev, O.; Kawi, S.; Deutsch, S. E.; Gates, B. C. *Nature* **1994**, *372*, 346.
(6) Alexeev, O.; Panjabi, G.; Gates, B. C. *J. Catal.* **1998**, *173*, 196.
(7) Maloney, S. D.; van Zon, F. B. M.; Kelley, M. J.; Koningsberger. D. C.; Gates, B. C. *Catal. Lett.* **1990**, *5*, 161.
(8) Zhao, A.; Gates, B. C. *J. Am. Chem. Soc.* **1996**, *118*, 2458.
(9) Alexeev, O.; Gates, B. C. *J. Catal.* **1998**, *176*, 310.
(10) Panjabi, G. Ph.D. Dissertation, University of California, Davis, CA, 2000.
(11) Kawi, S.; Gates, B. C. *Inorg. Chem.* **1992**, *31*, 2939.
(12) Argo, A. M.; Gates, B. C. *J. Phys. Chem. B* **2003**, *107*, 5519.
(13) Goellner, J. F. Ph.D. Dissertation, University of California, Davis, CA, 2000.
(14) Argo, A. M. Ph.D. Dissertation, University of California, Davis, CA, 2001.
(15) Xu, Z.; Gates, B. C. *J. Catal.* **1995**, *154*, 335.
(16) Odzak, J. F.; Argo, A. M.; Lai, F. S.; Gates, B. C. *Rev. Sci. Instrum.* **2001**, *72*, 3943.
(17) *Crystal Structures*, 2nd ed.; Wycoff, R. W. G., Ed.; Wiley: New York, 1963; Vol. 1, p 10.
(18) Coey, J. M. D. *Acta Crystallogr., Sect. B: Struct. Sci.* **1970**, *26*, 1876.
(19) Mason, R.; Rae, A. I. M. *J. Chem. Soc. A* **1968**, 778.
(20) Donnay, J. D. H.; Ondik, H. M. *Crystal Data Determinative Tables*, 3rd ed.; U.S. Department of Commerce, National Bureau of Standards and the Joint Committee on Powder Diffraction Standards: Washington, DC, 1973; Vol. II, p. C-4.
(21) Trömel, M.; Lupprich, E. *Z. Anorg. Allg. Chem.* **1975**, *414*, 160.
(22) Churchill, M. R.; Hutchinson, J. P. *Inorg. Chem.* **1978**, *17*, 3528.
(23) van Zon, F. B. M.; Maloney, S. D.; Gates, B. C.; Koningsberger, D. C. *J. Am. Chem. Soc.* **1993**, *115*, 10317.
(24) (a) Zabinsky, S. I.; Rehr, J. J.; Ankudinov, A.; Albers, R. C.; Eller, M. J. *Phys. Rev. B.* **1995**, *52*, 2995. (b) Ankudinov, A. Ph.D. Dissertation, University of Washington, 1996.
(25) Kirlin, P. S.; van Zon, F. B. M.; Koningsberger, D. C.; Gates, B. C. *J. Phys. Chem.* **1990**, *94*, 8439.
(26) Argo, A. M.; Gates, B. C. *Langmuir* **2002**, *18*, 2152.
(27) Argo, A. M.; Odzak, J. F.; Gates, B. C. *J. Am. Chem. Soc.* **2003**, *125*, 7107.
(28) Cortright, R. D.; Goddard, S. A.; Rekoske, J. E.; Dumesic, J. A. *J. Catal.* **1991**, *127*, 342.
(29) Goddard, S. A.; Cortright, R. D.; Dumesic, J. A. *J. Catal.* **1992**, *137*, 186.
(30) Rekoske, J. E.; Cortright, R. S.; Goddard, S. A.; Sharma, S. B.; Dumesic, J. A. *J. Phys. Chem.* **1992**, *96*, 1880.
(31) Horiuti, J.; Miyahara, K. *Hydrogenation of Ethylene on Metallic Catalysts*, NBS−NSRDS 13; U.S. Government Printing Office: Washington, DC, 1968.
(32) Neurock, M.; van Santen, R. A. *J. Phys. Chem. B* **2000**, *104*, 11127.
(33) Beeck, O. *Discuss. Faraday Soc.* **1950**, 118.
(34) Schuit, G. C. A.; van Reijen, L. L. *Adv. Catal.* **1958**, *10*, 242.
(35) Mohsin, S. B.; Trenary, M.; Robota, H. J. *J. Phys. Chem.* **1991**, *95*, 6657.
(36) Thorn, D. L.; Hoffman, R. J. *J. Am. Chem. Soc.* **1978**, *97*, 4445.
(37) Cremer, P. S.; Su, X.; Shen, Y. R.; Somorjai, G. A. *Catal. Lett.* **1996**, *40*, 143.
(38) Cremer, P. S.; Su, X.; Shen, Y. R.; Somorjai, G. A. *J. Am. Chem. Soc.* **1996**, *118*, 2942.
(39) Marinova, Ts. S.; Kostov, K. L. *Surf. Sci.* **1987**, *181*, 573.
(40) Beebe, T. P., Jr.; Yates, J. T., Jr. *J. Phys. Chem.* **1987**, *91*, 254.
(41) Vaarkamp, M.; Linders, J. C.; Koningsberger, D. C. *Physica B* **1995**, *209*, 159.